forum acusticum 2026
8-12 September · Graz, Austria

BUILDING WEB-PAGE BOUNDARY ELEMENTS SOFTWARE FOR MODELING SONIC CRYSTALS SCATTERING PATTERN

Marek Moszyński[1], Isabel Pérez Arjona[2], Víctor Espinosa Roselló[2]

[1] *Department of Geoinformatics, Gdańsk University of Technology, Poland*
[2] *Inst. d'Investigació per a la Gestió Integrada de Zones Costaneres, Universitat Politècnica de València, Spain*

This paper is a revised version of the authors' submitted manuscript that was peer-reviewed by at least two anonymous reviewers.

Abstract

The rapid development of computational acoustics has enabled the creation of digital twins for a wide range of engineering applications. Among the most versatile numerical approaches are the Finite Element Method (FEM) and the Boundary Element Method (BEM), both of which are now available in advanced commercial packages supporting full-scale acoustic design and verification.

However, innovative research concepts often require transparent and customizable tools that expose the underlying numerical formulation—capabilities that commercial software rarely provide. This motivates the use of programmable, open modeling environments that allow researchers to inspect, modify, and extend the core algorithms, particularly in BEM-based scattering analysis.

Building on our earlier contribution [1], this paper presents `mm-bem`, a lightweight web-browser application implementing a classical BEM formulation for acoustic scattering from mesh-defined objects. The tool runs entirely client-side, requires no installation, and provides interactive visualization of both near- and far-field responses. As a demonstration, we analyze the scattering behaviour of a periodic lattice of spheres, illustrating the applicability of the approach to sonic-crystal configurations.

Keywords: *boundary element method, sonic crystals, web-browser code*

1. Introduction

The development of computational acoustics over the past decades has enabled increasingly accurate numerical modelling of wave phenomena, including the behaviour of periodic structures such as photonic and sonic crystals. Early theoretical studies on sonic crystals in underwater acoustics—notably [2]–[4]—demonstrated how periodic impedance contrasts can give rise to diffraction suppression, band gaps, and other wave-guiding effects analogous to those observed in photonic materials.

In practical underwater applications, such periodicity can be introduced by embedding regions of strong acoustic contrast, for example by arranging voids or steel spheres within a fluid medium. Although the governing physics remains that of the standard acoustic wave equation, the presence of multiple scatterers with distinct material properties leads to complex interaction effects that require robust numerical tools for accurate prediction.

While commercial FEM and BEM packages provide powerful capabilities for full-scale acoustic analysis, they often lack the transparency and flexibility needed for exploratory research or for validating new modelling concepts. This motivates the development of lightweight, programmable environments that expose the underlying numerical formulation and allow researchers to inspect and modify each stage of the computation.

In this context, and as a continuation of our earlier contribution [1], the present work introduces `mm-bem`, a browser-based Boundary Element Method implementation designed for interactive acoustic scattering analysis. To illustrate its capabilities, we examine the scattering behaviour of a vacuum-filled sphere lattice immersed in water, demonstrating how the tool can be used to explore sonic-crystal configurations directly within a web environment.

2. Methods

To analyse the scattering behaviour of the sphere lattices introduced in the previous section, we adopt a classical Boundary Element Method (BEM) formulation for time-harmonic acoustics based on a direct boundary integral formulation. In an unbounded, homogeneous fluid medium, the total acoustic pressure

Corresponding author: *marek.moszynski@pg.edu.pl.*

field $p(\mathbf{x})$ is governed by the Helmholtz equation

$$\nabla^2 p(\mathbf{x}) + k^2 p(\mathbf{x}) = 0, \tag{1}$$

where $k = \frac{\omega}{c_0} = \frac{2\pi f_0}{c_0}$ is the acoustic wavenumber when considering a plane wave with frequency f_0 spreading in a medium with sound speed c_0. The total field is decomposed as

$$p(\mathbf{x}) = p_{\text{inc}}(\mathbf{x}) + p_{\text{scat}}(\mathbf{x}), \tag{2}$$

with p_{inc} the known incident field and p_{scat} the unknown scattered field. For a pressure-release (soft) scatterer, the total pressure vanishes on the boundary S:

$$p(\mathbf{x}) = 0, \qquad \mathbf{x} \in S. \tag{3}$$

By applying Green's second identity to the total pressure field $p(\mathbf{x})$ and the free-space Green function in the exterior domain (accounting for the Sommerfeld radiation condition for the scattered component), the total pressure at any exterior domain point $\mathbf{x}$ is expressed directly as

$$p(\mathbf{x}) = p_{\text{inc}}(\mathbf{x}) + \int_S \left[G(\mathbf{x},\mathbf{y}) \frac{\partial p(\mathbf{y})}{\partial n(\mathbf{y})} - p(\mathbf{y}) \frac{\partial G(\mathbf{x},\mathbf{y})}{\partial n(\mathbf{y})} \right] \mathrm{d}S(\mathbf{y}), \tag{4}$$

where $\mathbf{n}(\mathbf{y})$ is the unit normal vector pointing outwards from the scatterer surface into the fluid medium, and

$$G(\mathbf{x},\mathbf{y}) = \frac{e^{ik|\mathbf{x}-\mathbf{y}|}}{4\pi|\mathbf{x}-\mathbf{y}|} \tag{5}$$

is the free-space Green function. By defining the physical normal derivative of the total pressure as

$$p_n(\mathbf{y}) \equiv \frac{\partial p(\mathbf{y})}{\partial n(\mathbf{y})}, \tag{6}$$

and directly substituting the pressure-release condition (3) into Equation (4), the double-layer integral term drops out. Finally, taking the limit as the exterior point $\mathbf{x}$ approaches a point $\mathbf{x}_i$ on the boundary surface S, the total pressure $p(\mathbf{x}_i)$ on the left-hand side vanishes via (3), yielding the direct boundary integral equation:

$$\int_S q(\mathbf{y})\, G(\mathbf{x}_i,\mathbf{y})\, \mathrm{d}S(\mathbf{y}) = -\, p_{\text{inc}}(\mathbf{x}_i), \qquad \mathbf{x}_i \in S \tag{7}$$

where p_{inc} describes a plane wave coming from the θ, ϕ direction:

$$p_{\text{inc}}(\mathbf{x}_i) = e^{ik\left(\sin\theta\cos\phi\, x_i^{(1)} + \sin\theta\sin\phi\, x_i^{(2)} + \cos\theta\, x_i^{(3)}\right)} \tag{8}$$

with $\mathbf{x_i} = (x_i^{(1)}, x_i^{(2)}, x_i^{(3)})$. The surface S is partitioned into N flat triangular elements S_j with area $|S_j|$ and centroid $\mathbf{y}_j$. The normal derivative $q(\mathbf{y})$ is approximated as constant on each element:

$$p_n(\mathbf{y}) \approx p_{n,j} \qquad \mathbf{y} \in S_j. \tag{9}$$

Using a centroid-based approximation of the element integral (the standard piecewise-constant BEM formulation P_0 with centroid collocation and 1-point quadrature),

$$\int_{S_j} G(\mathbf{x}_i,\mathbf{y})\, \mathrm{d}S(\mathbf{y}) \approx G(\mathbf{x}_i,\mathbf{y}_j)\, |S_j|, \tag{10}$$

the discretized boundary equation becomes

$$\sum_{j=1}^{N} G(\mathbf{x}_i,\mathbf{y}_j)\, |S_j|\, p_{n,j} = -\, p_{\text{inc}}(\mathbf{x}_i). \tag{11}$$

To simplify the algebra and avoid explicit area factors in the field evaluation, we introduce the integrated flux

$$Q_j := |S_j|\, p_{n,j} \tag{12}$$

which could be interpreted as surface source strength. The boundary equation (11) then takes the compact form

$$\sum_{j=1}^{N} G(\mathbf{x}_i,\mathbf{y}_j)\, Q_j = -\, p_{\text{inc}}(\mathbf{x}_i), \qquad i = 1, \ldots, N. \tag{13}$$

The centroid rule (10) provides an accurate and efficient approximation for all off-diagonal terms where $\mathbf{x}_i \neq \mathbf{y}_j$. However, for the self-interaction diagonal terms ($i = j$), the collocation point $\mathbf{x}_i$ coincides with the element centroid $\mathbf{y}_i$, causing the Green's function kernel to exhibit a weak $1/r$ singularity as $r \to 0$. In this case, the 1-point quadrature fails, and the integral must be evaluated by isolating the singularity. To regularise the diagonal terms, the Helmholtz Green's function is decomposed into its singular Laplace part and a smooth, frequency-dependent remainder:

$$G(\mathbf{x}_i,\mathbf{y}) = \frac{1}{4\pi r} + \frac{e^{ikr} - 1}{4\pi r}, \qquad r = \|\mathbf{x}_i - \mathbf{y}\|. \tag{14}$$

When integrating (14) the integral of the first part of the right-hand side represents the purely geometric, singular static component. For a flat triangular element with centroid collocation, it can be integrated analytically. To make its scaling behavior explicit, we factor out the size of the element, yielding:

$$\int_{S_i} \frac{1}{4\pi r}\, \mathrm{d}S(\mathbf{y}) = \alpha_i = \tilde{\alpha}_i \sqrt{|S_i|}, \tag{15}$$

where $\tilde{\alpha}_i$ is a dimensionless shape coefficient that depends strictly on the aspect ratio and angles of the triangle S_i, but is independent of its physical scale. For a equilateral triangles ($|S_i| = \frac{\sqrt{3}}{4} l^2$) very often used by mesh generators with centroid collocation, this dimensionless factor evaluates analytically to $\tilde{\alpha}_i = \frac{\sqrt[4]{3}\ln(2+\sqrt{3})}{2\pi} \approx 0.2758$. For the second part, the integrand is bounded since $\lim_{r\to 0} \frac{e^{ikr}-1}{4\pi r} = \frac{ik}{4\pi}$. To preserve algebraic consistency with (11), the self-interaction terms ($i = j$) in the summation must be implicitly divided by the element area $|S_i|$, yielding the final regularised diagonal coefficient:

$$G(\mathbf{x}_i, \mathbf{y}_i) = \frac{\tilde{\alpha}_i \sqrt{|S_i|} + \frac{ik}{4\pi}|S_i|}{|S_i|} = \frac{\tilde{\alpha}_i}{\sqrt{|S_i|}} + \frac{ik}{4\pi}. \quad (16)$$

Equation (16) reveals that in this integrated-flux formulation, while the off-diagonal entries and the imaginary parts of the diagonal entries do not explicitly depend on the triangular element size, the real parts of the diagonal coefficients do. However, it is worth noting that when the standard engineering rule for mesh generation—restricting the edge length to the wavelength ($L \leq \lambda/10$)—is adopted, the element size becomes intrinsically linked to the frequency. Consequently, the real part effectively translates its dependence from the geometric area $|S_i|$ into a direct linear dependence on the wavenumber k.

This frequency-dependent regularization eliminates pure geometric grid dependencies, justifying the transition to meshless formulations, such as the Method of Fundamental Solutions (MFS) [5]–[7], where the explicit geometric grid dependencies are bypassed entirely. In the MFS framework, the singular boundary integral equation is replaced by a linear combination of fundamental solutions, which is regularised by offsetting the source points (or virtual nodes) away from the physical boundary into the fictitious exterior domain. Specifically, to maintain spectral stability and avoid the mathematical breakdown associated with the $1/r$ singularity, each source point $\mathbf{y}_i$ is generated by shifting the corresponding boundary collocation point $\mathbf{x}_i$ outward along the exterior unit normal vector $\mathbf{n}_i$ by a frequency-tuned distance of $d = \lambda/20$. By coupling this geometric offset directly to the wavelength via $\lambda = 2\pi/k$, the distance scales dynamically as $d = \pi/(10\,k)$, which ensures that the minimum distance between any collocation point and the virtual source grid shrinks in perfect lockstep with the wave contraction at higher frequencies. Consequently, this $\lambda/20$ normal regularisation prevents the kernel matrix from becoming highly ill-conditioned due to excessive proximity, while simultaneously avoiding the loss of high-frequency oscillatory resolution that occurs if the sources are placed too far from the boundary, thereby creating a robust and stable meshless framework for high-wavenumber Helmholtz scattering problems.

Both presented approaches leads to solving the same Eq. (13). Once the coefficients Q_j are computed, the scattered field at any point $\mathbf{x}$ in the exterior domain is obtained from

$$p_{\text{scat}}(\mathbf{x}) \approx -\sum_{j=1}^{N} G(\mathbf{x}, \mathbf{y}_j)\, Q_j. \quad (17)$$

Because the element area $|S_j|$ is absorbed into the unknown Q_j, no additional area factor appears in the field evaluation.

3. Implementation

The full `mm-bem` package is openly available to ensure reproducibility [8]. It includes source codes written in multiple programming languages and supports various BEM algorithms [9]. It uses i.e. FreeFem++ [10], Bempp [11] (Python) and gypsilab [12] (Matlab) frameworks. The web-based demonstration of `mm-bem` code is written in Javascript with C/WebAssembly SIMD128 optimized code and calculates acoustic scattering patterns from mesh-defined targets using the BEM equations presented in previous section. The BEM algorithm employs classical P0 elements. For comparison purposes the demonstration also includes an implementation of Method of Fundamental Solution (MFS) [13], which uses source points located inside the mesh along element normals at a distance of 0.05λ.

The demonstration application runs entirely within modern web browsers and computes scattering patterns for pressure-release (soft) targets represented by up to 20,000 triangular elements, a boundary imposed by the 4 GB memory address space limitation of current browser environments. The solver utilizes an LDL^T factorization [14], directly exploiting the complex symmetric property of the formulated equations. To alleviate the restriction on the maximum number of elements, an Adaptive Cross Approximation accelerated GMRES (ACA-GMRES) solver [15] is currently being implemented. This development necessitates porting the entire computational core to C/WebAssembly; while the existing JavaScript implementation is functional, it introduces severe performance and capacity bottlenecks due to high object allocation overhead rather than the structural density of the triangular mesh. The graphical user interface of the application is presented in Fig. 1. Notably, the tool requires no third-party libraries and can operate fully offline on any client architecture. Its primary purpose is to compute the far-field target strength (TS) of arbitrary geometries across multiple frequencies, provided that the standard wavelength-to-element-size resolution criterion is satisfied. Furthermore, the framework supports near-field evaluations within a user-defined volumetric region.

The *Input parameters* panel provides the interface for configuring simulations. Users may specify: (1) the target mesh, (2) the incident plane-wave direction angles θ_0 and ϕ_0, which are shifted by π relative to the conventional angles θ and ϕ to ensure geometric consistency for the backscattering direction, (3) the operating frequency f_0, and (4) the sound speed c_0 in water (adjustable in the *Configuration* section).

Target meshes can be selected from a dropdown menu containing several canonical examples, including multi-sphere configurations. The mesh is displayed in the *Data Visualisation* section on the left 3D panel, while the results of the BEM calculations appear in the right panel as a 2D polar plot of the scattering pattern. The near-field representation can be toggled on or off directly from the chart interface.

The frequency parameter may also be swept over a predefined range (up to 360 kHz). In this mode, results are visualized in the polar plot, where angular coordinates correspond to frequency values in kilohertz. Several illustrative examples are provided in the *Gallery* section.

To verify the implemented algorithms, the web application includes a built-in, scriptable mesh generator capable of producing simple target geometries, including a perfect sphere for which the exact analytical solution is known. This feature enables users to compare numerical results against theoretical calculations directly within an integrated 2D plotting interface. Consequently, it provides a reliable benchmark to rigorously evaluate the execution speed, numerical accuracy, and convergence characteristics of both the BEM and MFS formulations, as well as the performance of the LDL^T and ACA-GMRES solvers under the introduced regularization strategies. As an illustrative example, Fig. 2 presents a comparison of the scattering patterns obtained for a low-resolution sphere (128 triangles) and a medium-resolution sphere (512 triangles) against the exact analytical solution for a 1.905 cm sphere model at 38 kHz. It is worth noting that although the low-resolution mesh for that frequency does not satisfy the standard edge-length-to-wavelength resolution criterion, the computed numerical result remains remarkably close to the exact solution.

Users may also upload custom target meshes in one of the following formats: GMSH MSH 2.0 (triangular elements) or STL.

To demonstrate the practical applicability of the web-based framework for complex multiple-scattering environments, a sonic crystal experiment conducted in water ($c \approx 1480$ m/s) is simulated, utilizing a periodic lattice composed of pressure-release (soft) spheres with a radius of $a = 5.5$ mm (diameter 11.0 mm). At the operating frequency of $f = 38$ kHz, the acoustic wavelength in water evaluates to $\lambda = c/f \approx 38.95$ mm. Under these conditions, the geometric size of the spheres is smaller than the wavelength ($2a \approx 0.28\lambda$), placing the scatterers firmly within the coupled scattering regime.

To explore the wave-manipulation capabilities of this setup, two distinct lattice configurations are investigated. First, a standard benchmark is established using a sphere scatterer lattice with a lattice constant of $a_{\text{lat}} = 15$ mm. This spacing yields a significant filling fraction of $F = \frac{4}{3}\pi a^3/a_{\text{lat}}^3 \approx 20.66\%$, providing a strongly coupled periodic arrangement well-suited to evaluate the formation of directional bandgaps and classic multiple-scattering reflections. Second, an acoustic lens sonic crystals configuration, where the spatial positions of the spheres are tailored to form a curved, lens-shaped lattice. This non-uniform distribution is designed to focus the transmitted acoustic energy into a localized focal spot. Simulating these intricate multi-body arrays under the $\lambda/10$ resolution criterion provides a highly demanding computational

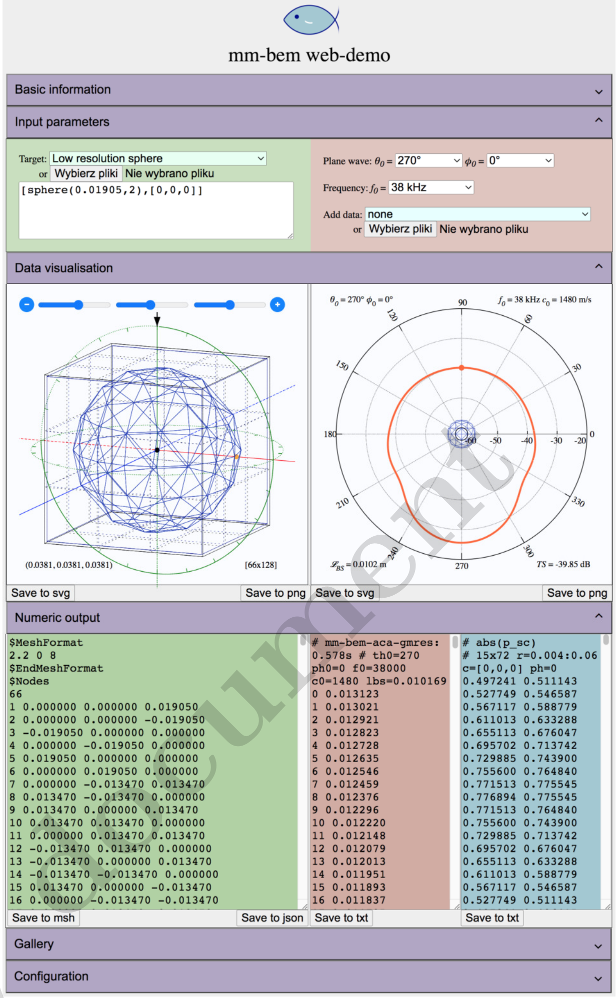

Figure 1: Initial view of mm–bem web–demo showing calculation of scattering function at 38kHz for low resolution soft sphere with radius equal to 1.905cm represented by 66 nodes and 128 triangular elements.

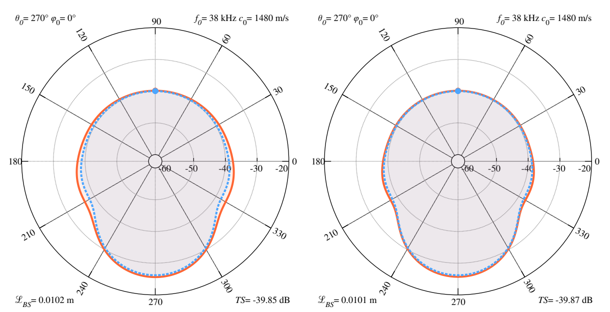

Figure 2: Comparison of the scattering patterns obtained for a low-resolution (left) and a medium-resolution (right) mesh model of a 1.905 cm pressure-release sphere at 38 kHz against the exact analytical solution (dashed blue curve). The backscattering direction is oriented towards the top of the polar plot.

environment, ideal for showcasing the efficiency and

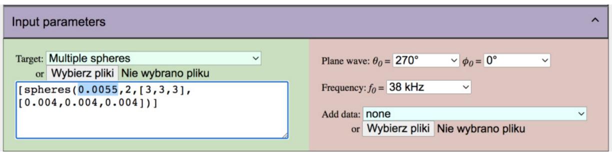

Figure 3: The definition of multiple sphere lattice by `spheres` buildin object.

accuracy of the developed solvers under intense wave interactions.
The Gallery section of mm–bem web–demo contains results in the form of figures for several use–cases. In this paper, those related to sonic crystals design are presented. To exemplify, Fig. 4 shows 3x3x3 lattice of low-resolution spheres with radius equal to 5.5 mm separated by 4 mm along with its far field pattern (red curve) and near field pattern (circular image) concentrated around lattice center as presented in 5. To achieve sonic crystal focusing it is required to design the lattice that contains more spheres. Hence the Fig. 6 shows user defined 10x5x10 sphere lattice with the same size and the same gap and resulting pattern with focusing at the distance of 24 cm. It is worth to be aware that such setup defines the problem with 64000 degrees of freedom as the low-resolution sphere in the system are represented by 128 elements. The Fig. 7 shows results obtained for the acoustics lens formation of the same sphere setup.

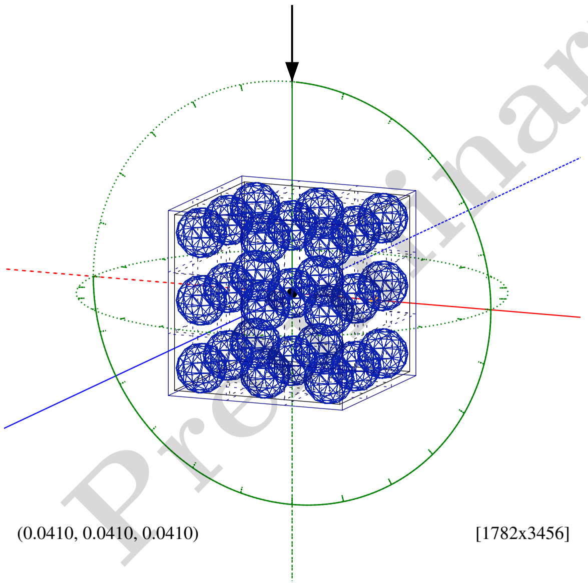

Figure 4: The mm-web visualisation of mesh representing 3x3x3 lattice constructed from 5.5 mm spheres separated by 4mm.

4. Conclusion

The `mm-bem` web demonstration illustrates that a complete boundary-element environment for sonic

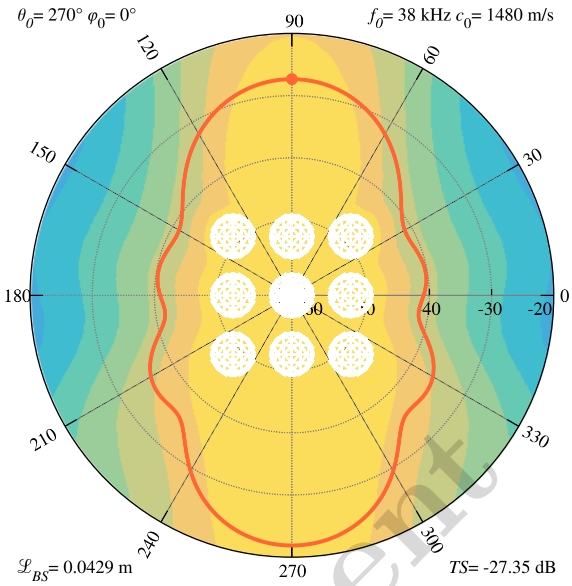

Figure 5: The near and far scattering pattern at 38kHz for the mesh model representing 3x3x3 sphere lattice shown in Fig. 4 presented in 2D view

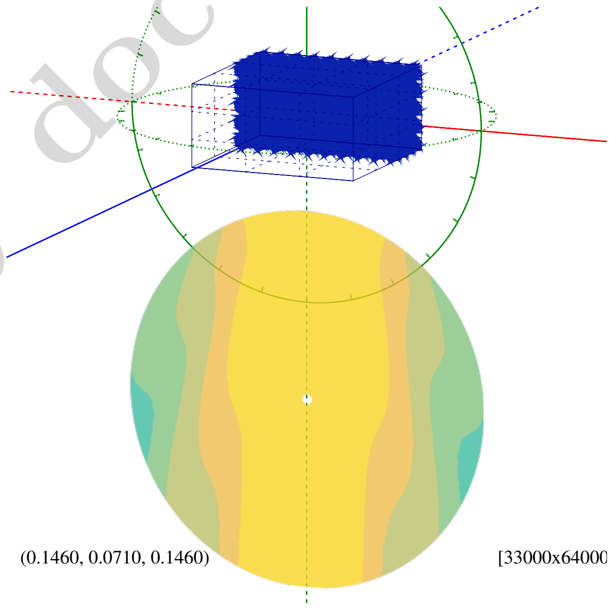

Figure 6: The near field scattering pattern at 38kHz for the mesh model representing 10x5x10 sphere lattice presented in 3D view.

crystals acoustics can be delivered as a lightweight, installation-free application. By relying solely on open web standards—with no external libraries, frameworks, or platform-specific dependencies—the tool remains portable, transparent, and cost-free, while operating seamlessly across platforms, including fully offline use. Its single-file architecture integrates example configurations and a gallery of reference results, enabling reproducible experimentation without auxiliary soft-

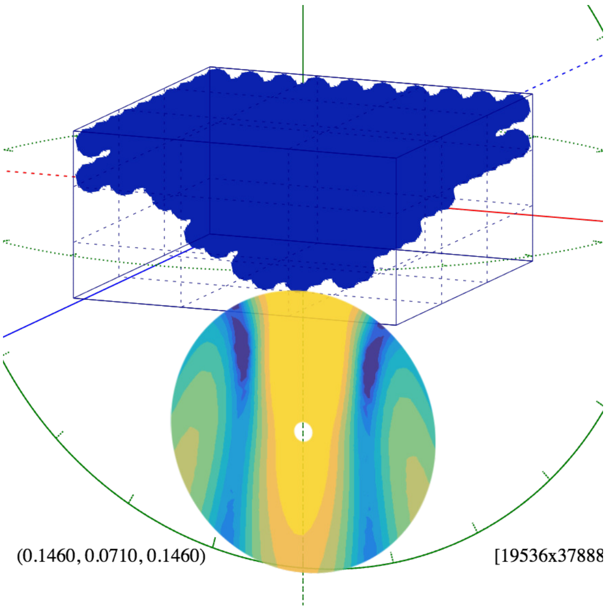

Figure 7: The near field scattering pattern at 38kHz for the mesh model representing acoustic lens formed from pressure-release sphere lattice.

ware.

Despite its minimal footprint, the system provides capabilities typically associated with larger scientific environments. These include text-based 3D input and 2D/3D output, publication-quality visualization through an embedded 3D viewer and polar-plot module, and support for merging multiple mesh files. The tool also offers mesh-generation scripting, including an exact-sphere calculator.

Together, these features demonstrate that modern browser technologies are sufficient to host a compact yet expressive BEM environment. The result is a portable research and teaching tool that lowers the barrier to experimentation, encourages transparent workflows, and highlights the potential of pure, standards-based code for scientific computing.

References

[1] M. Moszyński, I. Pérez Arjona, and V. Espinosa Roselló, "Using open software modeling tools for innovative transducer designs," in *Proceedings of Forum Acusticum Euronoise 2025*, D. de la Prida, J. Ramis, and M. Machimbarrena, Eds., Malaga, Spain, 2025, ISBN: 978-84-87985-35-5.

[2] V. Espinosa, V. J. Sánchez-Morcillo, K. Staliunas, I. Pérez-Arjona, and J. Redondo, "Subdiffractive propagation of ultrasound in sonic crystals," *PHYSICAL REVIEW*, vol. B 76, 140302(R), 2007.

[3] I. Pérez-Arjona, V. J. Sánchez-Morcillo, J. Redondo, V. Espinosa, and K. Staliunas, "Theoretical prediction of the nondiffractive propagation of sonic waves through periodic acoustic media," *PHYSICAL REVIEW*, vol. B 75, p. 014 304, 2007.

[4] V. J. Sánchez-Morcillo, K. Staliunas, V. Espinosa, I. Pérez-Arjona, J. Redondo, and E. Soliveres, "Propagation of sound beams behind sonic crystals," *PHYSICAL REVIEW*, vol. B 80, p. 134 303, 2009.

[5] G. Fairweather and A. Karageorghis, "The method of fundamental solutions for elliptic boundary value problems," *Advances in Computational Mathematics*, vol. 19, no. 1, pp. 131–147, 2003.

[6] A. Barnett and T. Betcke, "Stability and convergence of the method of fundamental solutions for helmholtz problems on analytic domains," *Journal of Computational Physics*, vol. 227, no. 14, pp. 7003–7026, 2008.

[7] C. J. S. Alves and P. R. S. Antunes, "The method of fundamental solutions applied to helmholtz eigenvalues and source reconstruction," *Journal of Computational and Applied Mathematics*, vol. 180, no. 2, pp. 291–304, 2005.

[8] M. Moszynski, *Mm-bem web-demo*, `https://marmoszy.github.io/mm-bem`, Source code repository available at: `https://github.com/marmoszy/mm-bem/` (Accessed: 2026-07-15), 2026.

[9] M. Moszyński, I. Pérez Arjona, V. Espinosa Roselló, and A. Ladino Velásquez, "Using open fem/bem software for modeling fish target strength," in *Proceedings of the Underwater Acoustics Conference (UAC 2025)*, 2025.

[10] F. Hecht, "New development in freefem++," *Journal of Numerical Mathematics*, vol. 20, no. 3–4, pp. 251–265, 2012.

[11] T. Betcke and M. W. Scroggs, "Bempp-cl: A fast python-based just-in-time compiling boundary element library," *Journal of Open Source Software*, vol. 6, no. 59, 2021.

[12] F. Alouges and M. Aussal, "Fem and bem simulations with the gypsilab framework," *SMAI Journal of Computational Mathematics*, vol. 4, pp. 297–318, 2018.

[13] W. Chen and A. Karageorghis, "The method of fundamental solutions for three-dimensional helmholtz problems," *Applied Mathematical Modelling*, vol. 33, no. 1, pp. 374–390, 2009.

[14] G. H. Golub and C. F. Van Loan, *Matrix Computations*, 4th. Baltimore, MD, USA: Johns Hopkins University Press, 2013.

[15] I. B. A. Brancati M. H. Aliabadi, "Hierarchical adaptive cross approximation gmres technique for solution of acoustic problems using the boundary element method," *Computer Modeling in Engineering & Sciences*, vol. 43, no. 2, pp. 149–172, 2009, ISSN: 1526-1506.